Supplementary Information for:

Frequent floods in the European Alps coincide with cooler periods of the past 2500 years

Lukas Glur[1*°], Stefanie B. Wirth[2°], Ulf Büntgen[3,4,5], Adrian Gilli[2], Gerald H. Haug[2], Christoph Schär[6], Jürg Beer[1] and Flavio S. Anselmetti[1,4,‡]

[1]Swiss Federal Institute of Aquatic Science and Technology (Eawag), CH-8600 Dübendorf, Switzerland.

[2]Geological Institute, ETH Zurich, CH-8092 Zürich, Switzerland.

[3]Swiss Federal Institute for Forest, Snow and Landscape Research (WSL), CH-8903 Birmensdorf, Switzerland

[4]Oeschger Centre for Climate Change Research OCCR, CH-3012 Bern, Switzerland

[5]Global Change Research Centre AS CR, 60300 Brno, Czech Republic

[6]Institute for Atmospheric and Climate Science, ETH Zurich, CH-8092 Zürich, Switzerland

*Correspondence to: lukas.glur@eawag.ch

‡Present address: Institute of Geological Sciences, University of Bern, CH-3012 Bern, Switzerland

°These authors contributed equally to this work.

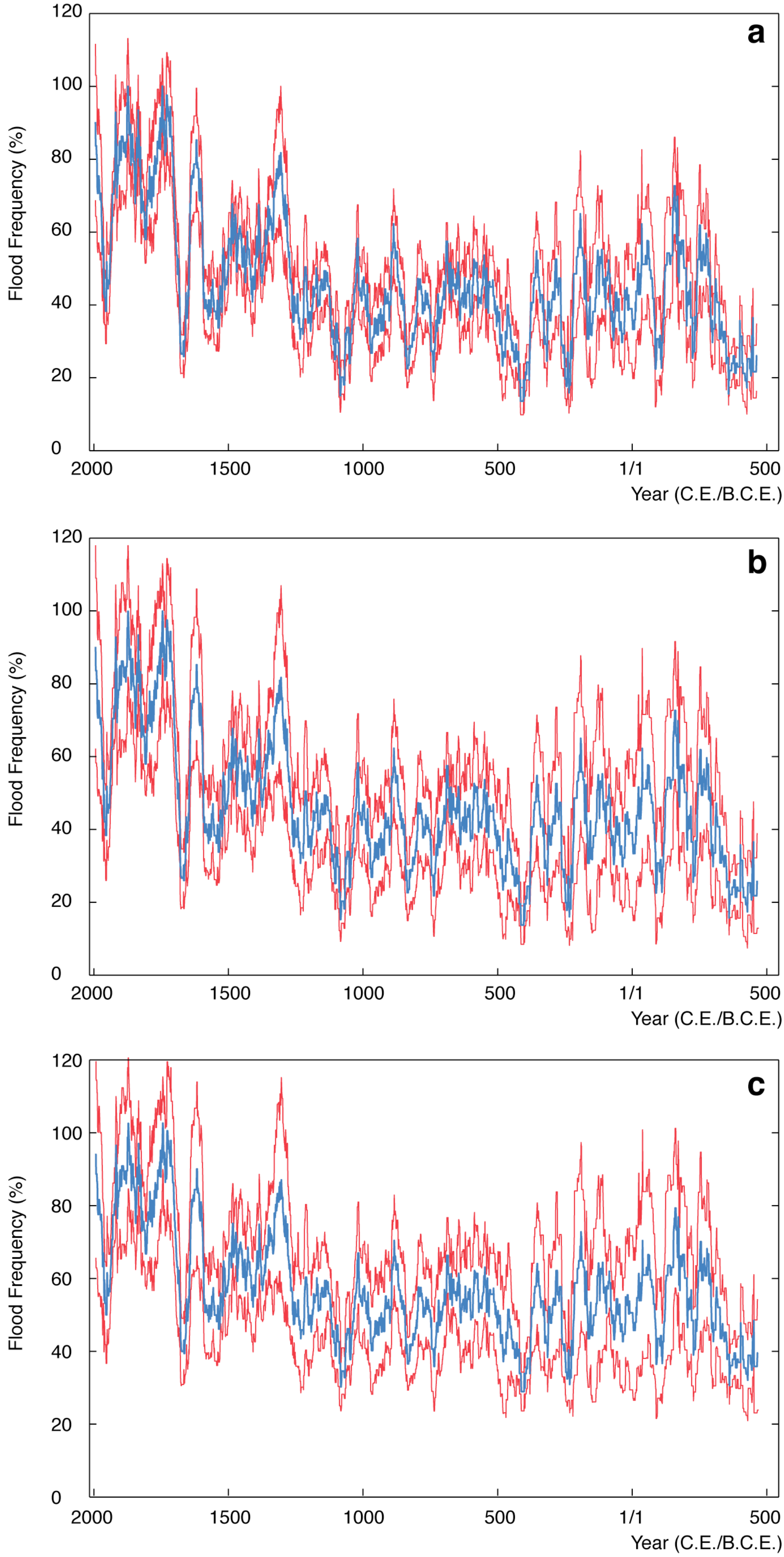
a
b
c
Flood Frequency (%)
0
20
40
60
80
100
120
2000
1500
1000
500
1/1
500
Year (C.E./B.C.E.)

Supplementary Figure S1 | Robustness of Central Alpine flood reconstruction. Compiled flood reconstruction (blue line) illustrated with 95% confidence interval (red lines) calculated from Alpine flood reconstructions omitting one (a), two (b) or three (c) lake records for every compilation (Jackknife analysis).

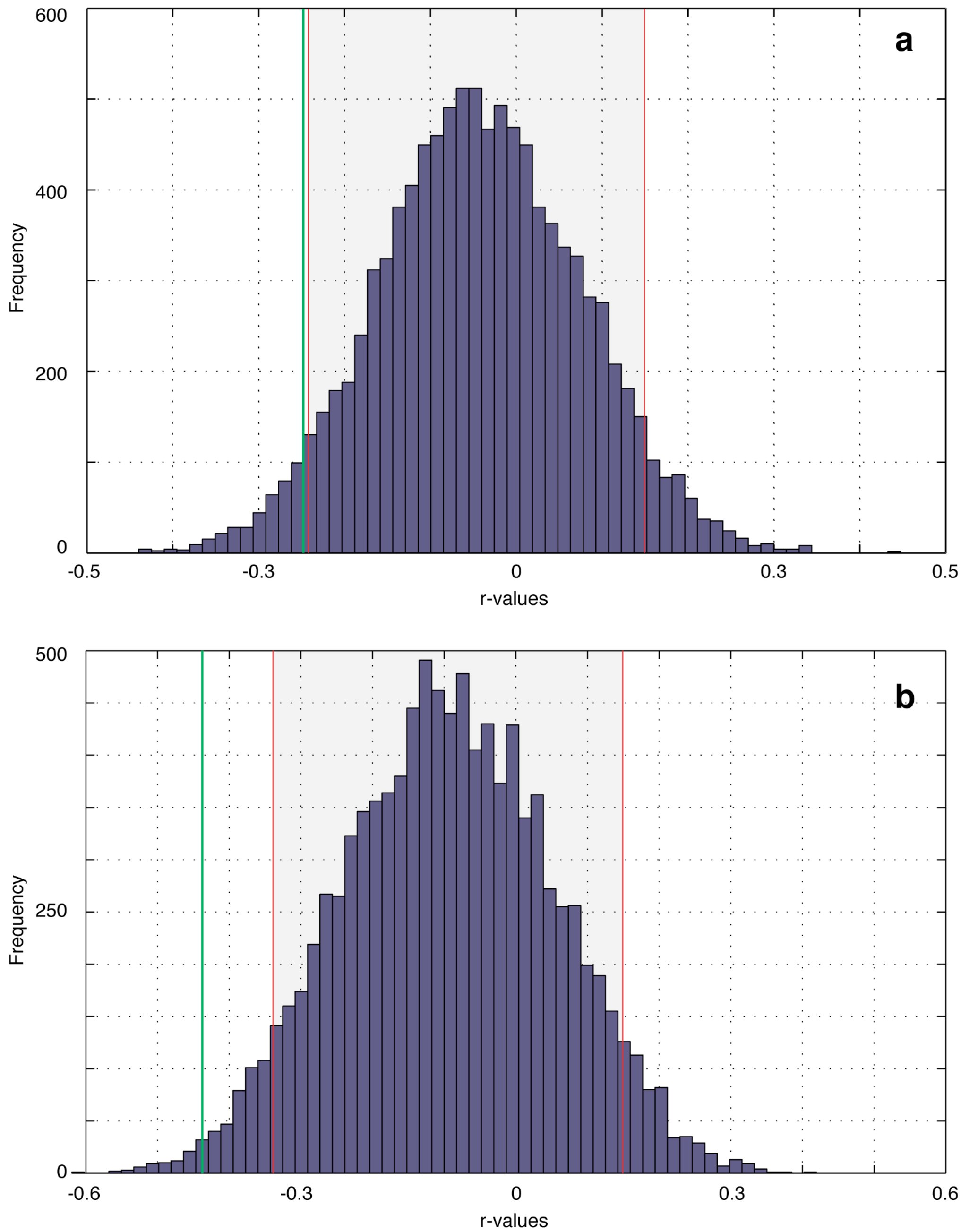

Supplementary Figure S2 | R-value distribution of the correlation between summer temperature reconstruction[21] and 10 000 randomized composite frequency curves. Red lines illustrate the 95% confidence interval of r-values of the correlation between the randomized composite frequency curves and the summer temperature reconstruction over 2500 a) and 1300 b) years. Each randomized frequency curve compromises 10 sites with randomized and re-shuffled events. Green lines indicate the r-value of the anti-correlation between the Central Alpine flood reconstruction and the summer temperature reconstruction.

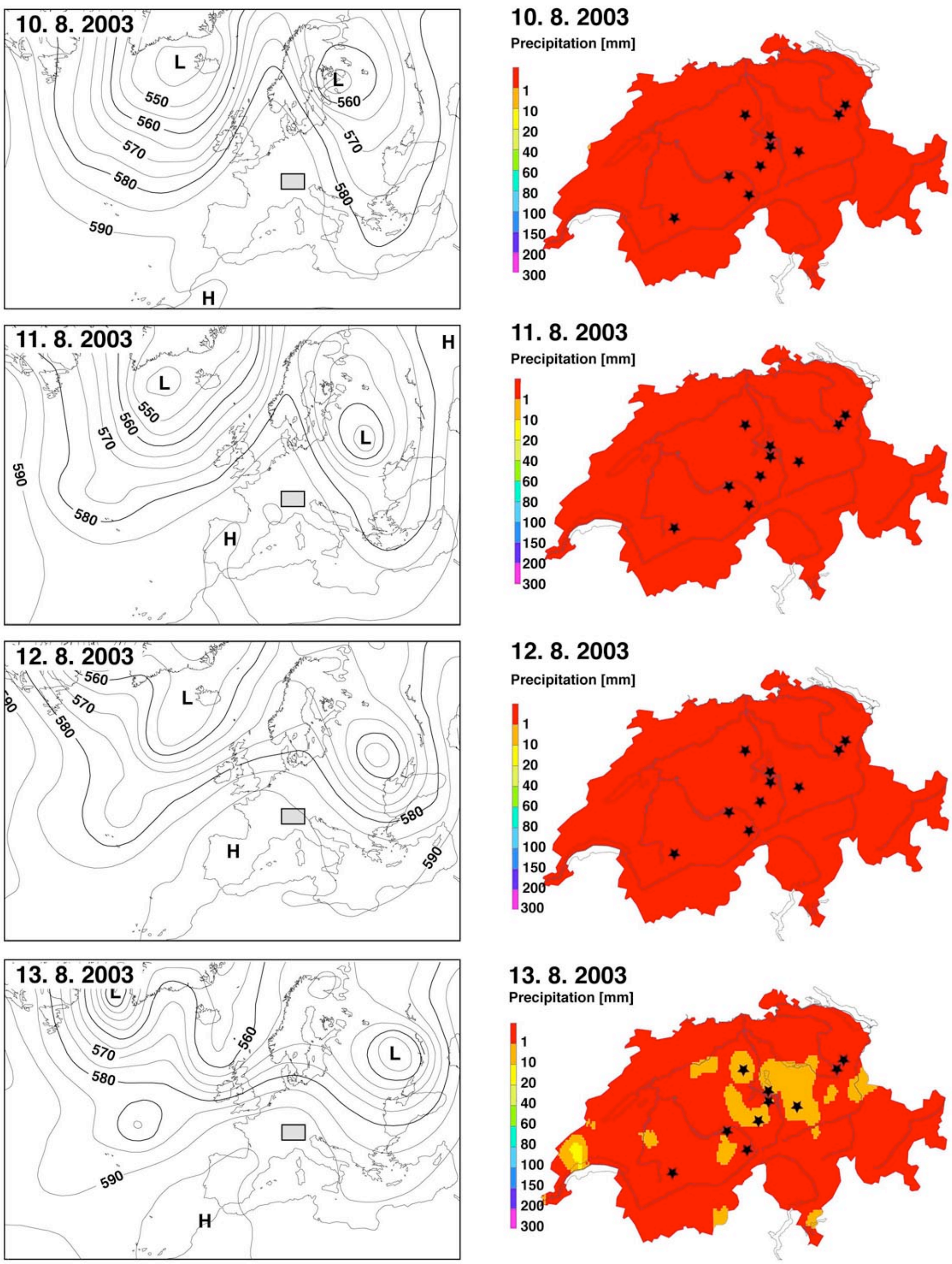

Supplementary Figure S3 | (Left) Daily mean of 500 hPa geopotential pressure levels during heat wave (2003) in Central Europe established online with ECMWF ERA-Interim reanalysis[32]. A high-pressure system dominates the Alpine area and shifts the westerly storm tracks poleward. Grey rectangle indicates Alpine study area. **(Right)** Gridded daily precipitation values in the study area. Maps are created with the ArcGIS® software by Esri using instrumental daily precipitation data provided by swisstopo[33]. Stars indicate studied lake sites. Map of Switzerland reproduced with permission of swisstopo / JA100119.

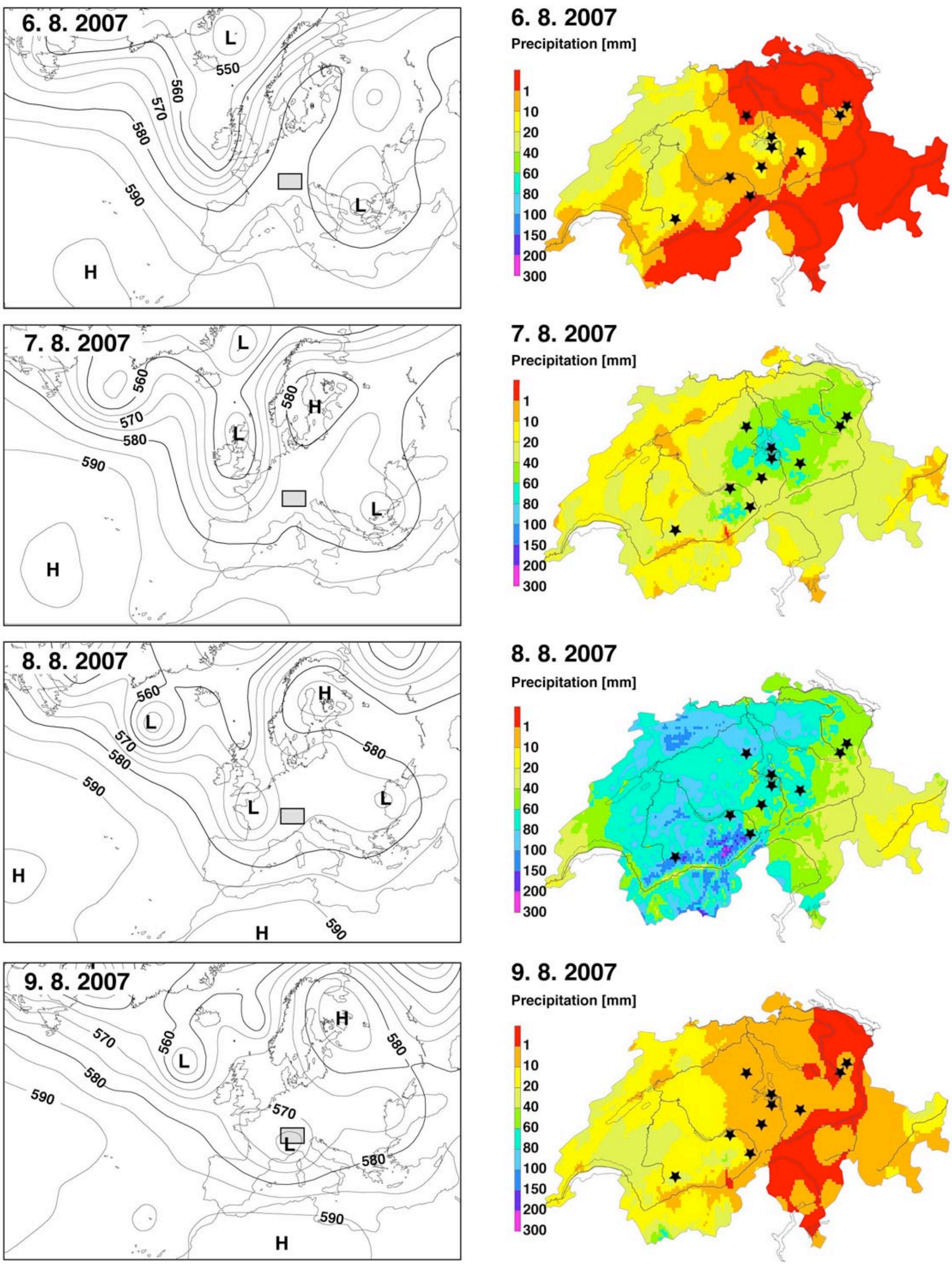

Supplementary Figure S4 | (Left) Daily mean of 500 hPa geopotential pressure levels during intense precipitation in the Swiss Alps caused by westerly storm tracks in 2007 established online with ECMWF ERA-Interim reanalysis[32]. Grey rectangle indicates Alpine study area. **(Right)** Gridded daily precipitation values in the study area. Maps are created with the ArcGIS® software by Esri using instrumental daily precipitation data provided by swisstopo[33]. Stars indicate studied lake sites. Map of Switzerland reproduced with permission of swisstopo / JA100119.

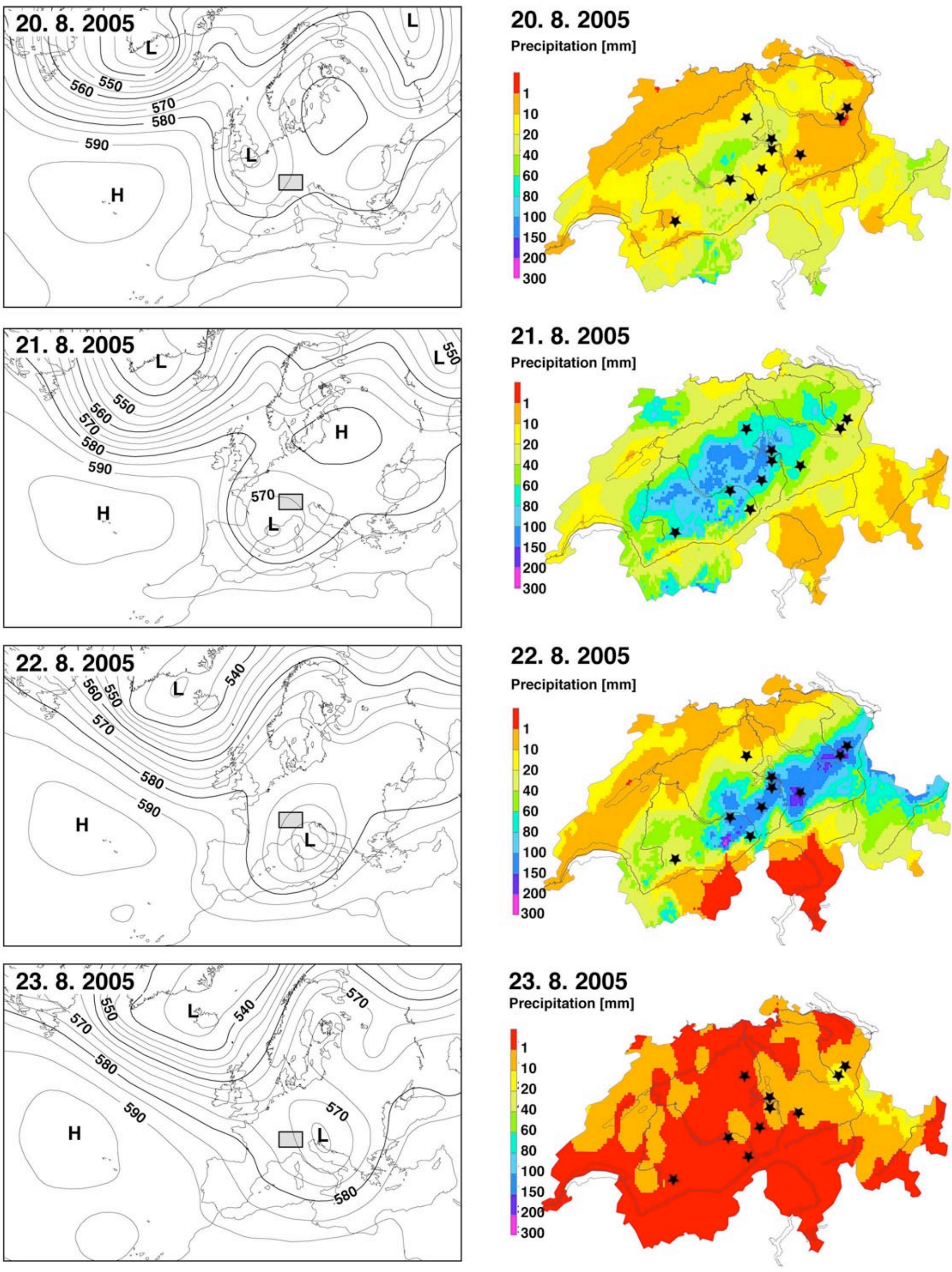

Supplementary Figure S5 | (Left) Daily mean of 500 hPa geopotential pressure levels during intense precipitation in the Swiss Alps caused by Vb circulation track in 2005 established online with ECMWF ERA-Interim reanalysis[32]. Grey rectangle indicates Alpine study area. **(Right)** Gridded daily precipitation values in the study area. Maps are created with the ArcGIS® software by Esri using instrumental daily precipitation data provided by swisstopo[33]. Stars indicate studied lake sites. Map of Switzerland reproduced with permission of swisstopo / JA100119.

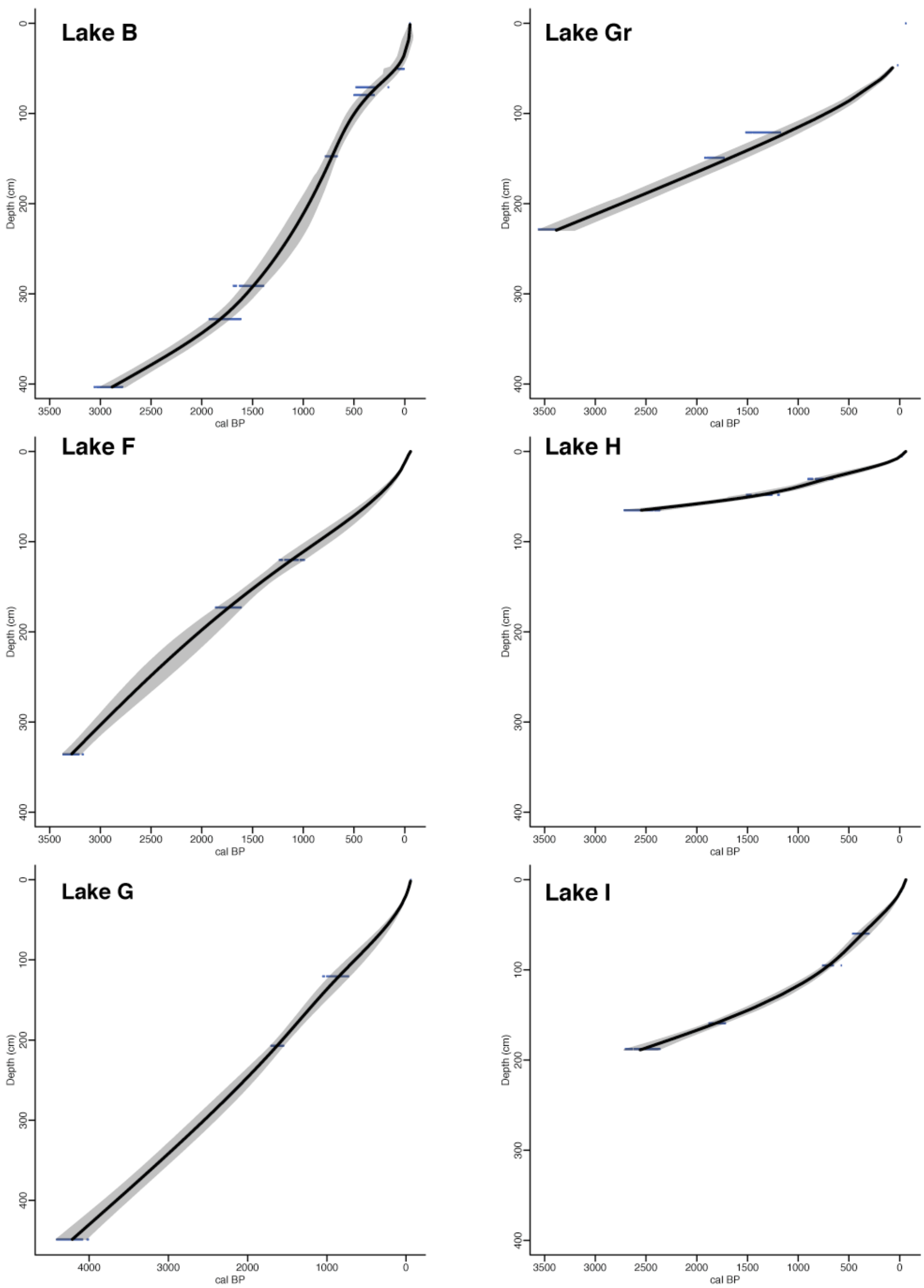

Supplementary Figure S6 | Graphs of age-depth models of lakes B, F, G, Gr, H and I Age-depth models are based on ^{137}Cs dating and AMS radiocarbon ages. Age-depth modeling was carried out applying spline interpolation between the dating points using the Clam software[31]. The grey area indicates 2σ ranges of age models.

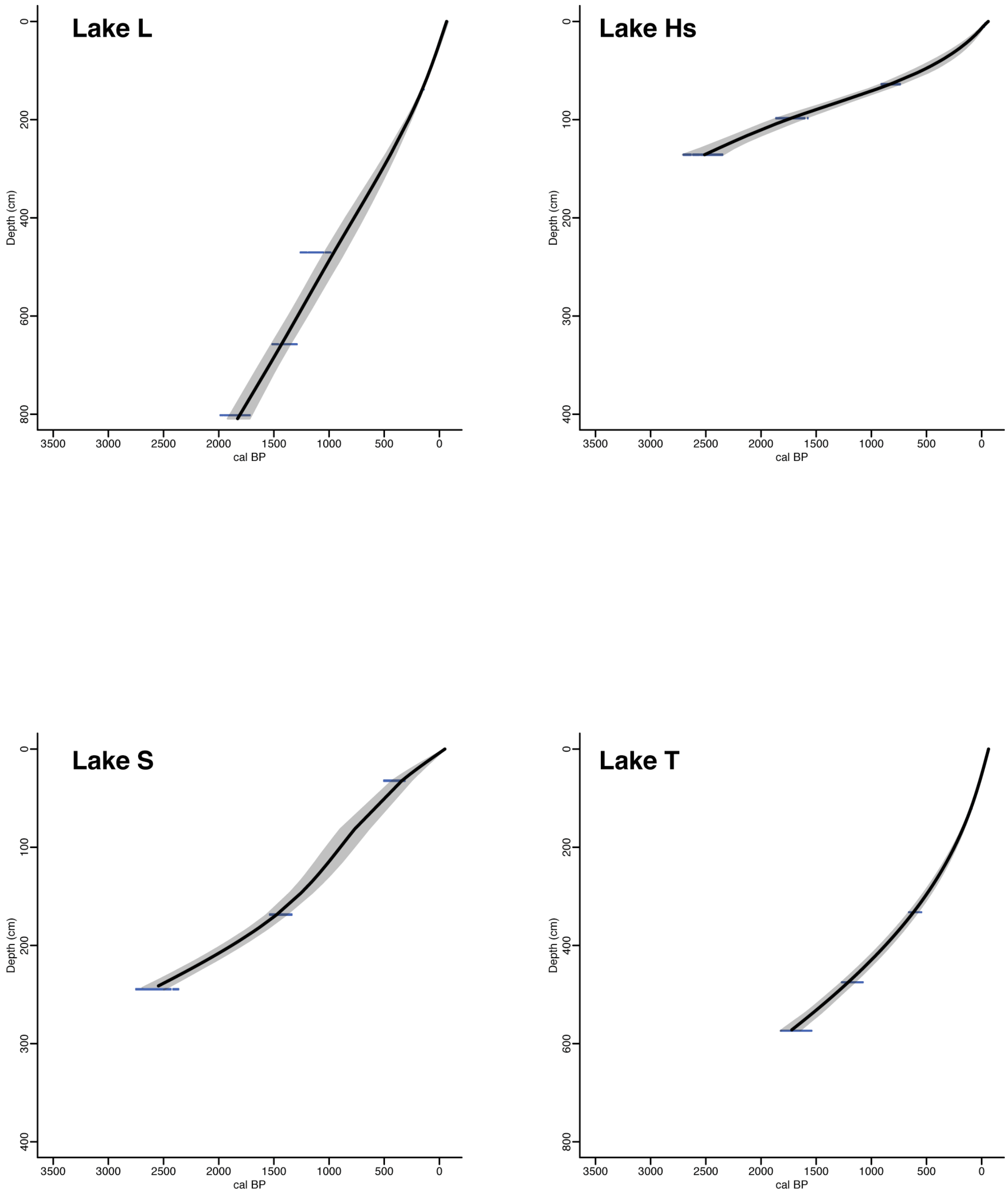

Supplementary Figure S7 | Graphs of age-depth models of lakes L, S, Hs and T

Age-depth models are based on ^{137}Cs dating and AMS radiocarbon ages. Age-depth modeling was carried out applying spline interpolation between the dating points using the Clam software[31]. The grey area indicates 2σ ranges of age models.

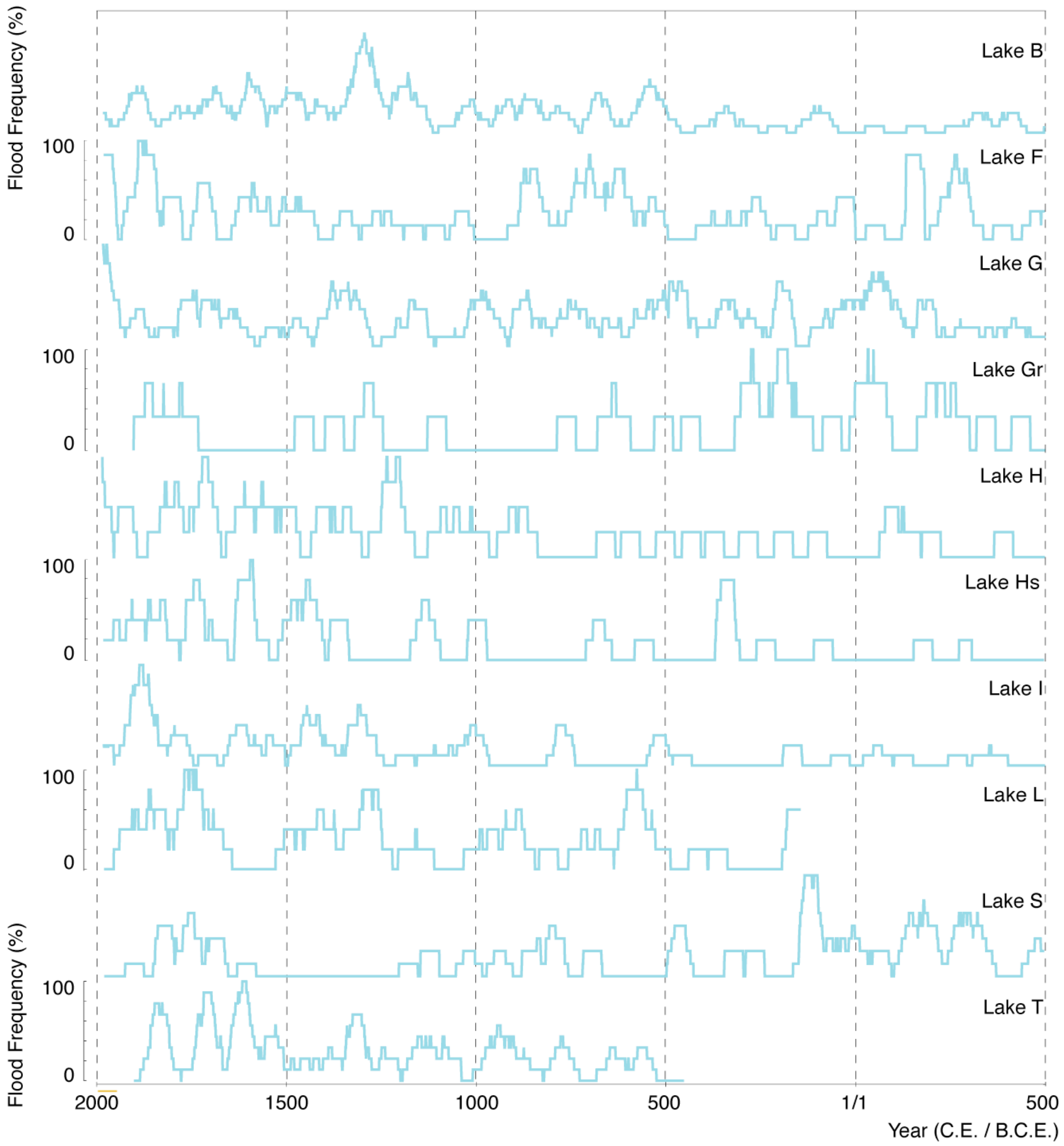

Supplementary Figure S8 | Flood frequency records of all studied lakes. Flood frequencies are presented as a 50-year moving sum of events normalized to 0 to 100%.

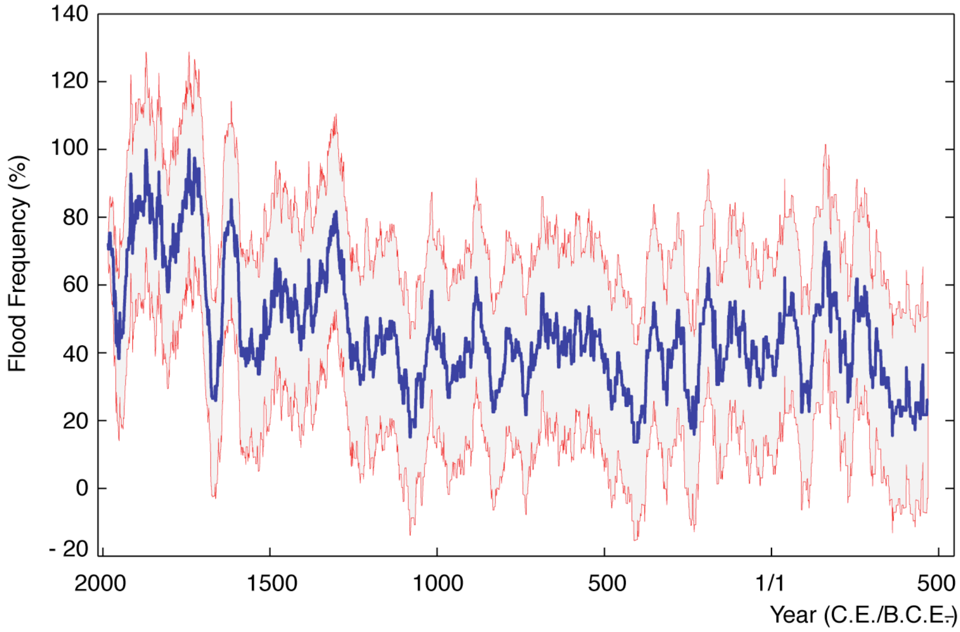

Supplementary Figure S9 | Significance test of Central Alpine flood reconstruction. Compiled flood reconstruction (blue line) illustrated with 95% confidence interval (red lines) of 10 000 frequency curves calculated from randomized event series. Each randomized frequency curve compromises 10 sites with randomized and re-shuffled events and was generated the same way as the Central Alpine flood reconstruction (Fig. 3).

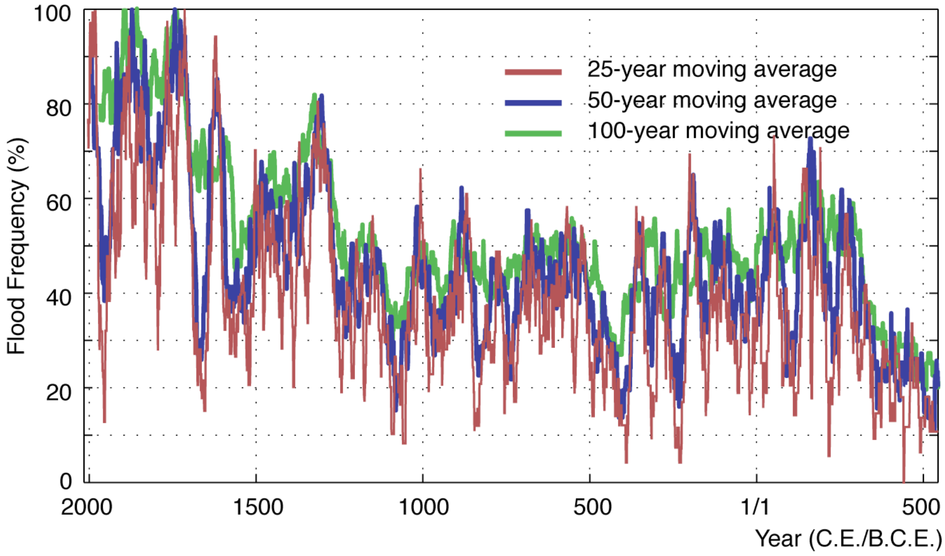

Supplementary Figure S10 | Effect of different window sizes on moving average curves of Central Alpine flood reconstruction. The main peaks and the general flood pattern seem not to be affected by changing window sizes.

Supplementary Table S1 | Characteristics of studied lakes.

Lake name (label)	Altitude (m.a.s.l.)	Surface area (km^2)	Catchment area (km^2)	Reconstructed flood interval	Number of flood layers
Baldegg (B)	463	5.2	73	2002 C.E. to 500 B.C.E.	150
Faelen (F)	1446	0.12	5.1	2009 C.E. to 500 B.C.E.	100
Glattalp (G)	1850	0.2	6.8	2011 C.E. to 500 B.C.E.	162
Grimsel (Gr)	1908	2.7	96.4	1930 C.E. to 500 B.C.E.	32
Hinterburg (H)	1514	0.05	1.62	2010 C.E. to 500 B.C.E.	50
Hinterer Schwendisee (Hs)	1159	0.012	5	2009 C.E. to 500 B.C.E.	42
Iffig (I)	2065	0.1	4.6	2010 C.E. to 500 B.C.E.	69
Lauerz (L)	447	3	69	2004 C.E. to 70 B.C.E.	54
Seelisberg (S)	740	0.18	2.8	2004 C.E. to 500 B.C.E.	76
Trueb (T)	1766	0.27	6.2	1920 C.E. to 450 C.E.	107

Supplementary Table S2 | AMS radiocarbon ages for all lake records.

Radiocarbon ages were calibrated using the IntCal09 calibration curve[34].

Sample ID	Lake label	Composite depth (cm)	Composite depth without event deposits (cm)	Conventional radiocarbon Age (BP)	± 1 σ	2σ age range of calibrated radiocarbon ages (BP)
UZ-4904	B	79	70.8	300	45	278-351
UZ-4905	B	89.6	79.5	335	55	313-396
UZ-4903	B	175.7	147.4	785	45	681-790
UZ-4690	B	352.5	291	1625	55	1433-1628
UZ-4691	B	402	327.9	1850	65	1631-1867
UZ-4729	B	483.4	403.2	2800	50	2757-2898
ETH-39519	F	150.1	120.2	1190	35	989-1237
ETH-39523	F	214.8	172.9	1805	45	1611-1865
ETH-39520	F	415.6	335.8	3065	35	3169-3369
ETH-44207	G	151.7	120.5	960	75	726-1052
ETH-44205	G	292.9	207.1	1715	35	1545-1705
ETH-45030	G	671	448.8	3815	55	4011-4413
ETH-41797	Gr	138.5	120.9	1410	80	1175-1518
ETH-41798	Gr	174.1	149.1	1895	35	1730-1922
ETH-41799	Gr	281.3	228.4	3230	45	3372-3561
UA-14630	H	77.7	30.4	805	60	660-905
UA-14631	H	171.1	47.9	1425	60	1188-1511
ETH-42027	H	205.4	65.1	2475	40	2364-2716
ETH-38342	Hs	185.6	63.6	900	30	739-910
ETH-39878	Hs	238.6	98.5	1800	50	1605-1865
ETH45158	Hs	300.8	135.7	2425	50	2349-2703
POZ-45473	I	96.3	59.8	310	30	301-466
ETH-41795	I	143.7	95	755	40	653-743

POZ-45472	I	218.4	159.2	1870	35	1717-1882
POZ-39380	I	251.7	187.8	2460	30	2363-2705
ETH-32360	L	562	470.5	1195	45	985-1260
ETH-32361	L	606	492	2195	45	2068-2337 +
ETH-32472	L	799.5	657.5	1470	55	1291-1516
ETH-32462	L	960	802	1910	55	1718-1986
UZ-4649	S	57	32.2	365	50	311-504
UZ-4935	S	160	155	555	55	510-654 +
UZ-4809	S	224	168.6	1545	50	1336-1539
UZ-4735	S	238	181.1	2265	50	2152-2351 +
UZ-4804	S	341	244.6	2525	65	2365-2752
ETH-42680	T	362.8	332.4	620	40	546-662
ETH-42683	T	529.1	475	1245	35	1075-1270
ETH-42681	T	641.6	573.8	1760	60	1541-1822
ETH-42908	T	784.5	703.4	2515	35	2471-2742 +

+ Discarded date: sample material derives from mass-movement deposits.

Supplementary notes

- Lake selection

Several criteria for the selection of lake sites potentially providing sensitive flood records were applied (Supplementary Tab. S1) (see also ref[13] for detailed discussion). i) The lake catchments have to be characterized by a high relief in order to enable the transport of eroded sediment particles to the downstream lake during heavy precipitation events. ii) Preferably, the lake inflows are only active during flood events. This facilitates the differentiation between flood deposits and authigenic background sediments. iii) The lake basins should have a well-defined depositional center, where the flood deposits material is accumulated. Sediment coring at this location allows retrieving continuous sediment sequences and, therefore, complete flood records.

- Age models

For age-depth modeling, event deposits, such as mass-movement-related and flood-related event layers, were removed from the sediment sequence as they were deposited very rapidly (hours to days). Age-depth models are based on ^{137}Cs and radiocarbon age horizons and were established using the Clam software[31] and the IntCal09 calibration curve[34]. Resulting age uncertainties (2σ-ranges) of the calibrated radiocarbon ages range between +/- 36 and +/- 201 years. The age of every flood layer was determined (Fig. 3a) by applying the spline interpolation between age horizons implemented in the Clam software[31] (Supplementary Figs. S6 and S7). The resulting age uncertainty (2σ-ranges) of individual flood deposits ranges between +/- 2 and +/- 175 years.

- Jackknife analyses

In order to test the robustness of the compiled Alpine flood reconstruction against a potentially only local signal of individual lake records, a Jackknife analysis was performed. First, the individual flood records were compiled to Alpine flood chronologies by omitting one lake record for each compilation. This test revealed 10 flood compilations containing 9 lake records each. The Central Alpine flood reconstruction was then plotted together with the 2σ standard deviation of these routines (Supplementary Fig. S1). The influence of outliers from single lakes flood record affecting the overall signal seems minor, which is expressed by the 2σ standard deviation ranging between 2 and 23 %. Afterwards, the Jackknife analysis was also performed omitting 2 and 3 lakes, respectively. The variability of the flood frequency curves increases when performing the Jackknife analysis omitting 2 and 3 lakes, which is expressed by increased 2σ standard deviations ranging from 2 to 30% and 2 to 35%, respectively.

- Recent examples of atmospheric conditions and their effects on Alpine precipitation

Common circulation patterns over the North Atlantic and Europe, which do favor/impede the occurrence of intense precipitation events in the Alps, show typical characteristics at 500 hPa geopotential pressure levels as discussed using the following examples based on instrumental data:

(1) In August 2003, Central Europe was under the influence of a strong high-pressure system[35]. Under this weather situation, Central Europe has suffered its hottest summer for at least 500 years and temperatures in Switzerland were topping the previous record by 2.4 °C[36]. During this year, the Alps experienced prolonged drought and heat and the entire summer period was characterized by a lack of convective rainfall in

many parts of Europe. This situation is projected to occur more frequently in the future[35] (Supplementary Fig. S3).

(2) In contrast, from August 6-9, 2007, the Alps were affected by strong westerly storm tracks that led to intense precipitation due to orographic rainfall mainly north of the central Alpine divide[7]. Consequentially, severe floods were recorded in the Alpine region. This specific weather situation was characterized by a weak Azores high-pressure system in a southerly position and a strong pressure gradient at mid-latitudes, generating strong westerly winds (Supplementary Fig. S4).

(3) A further extreme weather situation, referred to as 'Vb storm track', was observed from August 20-23, 2005, causing intense precipitation and severe flooding in the Northern Alpine region[19,37]. This Vb storm track was characterized by a low-pressure system travelling from the Mediterranean Sea northeastward. As in 2007, this weather situation was accompanied by a weak and southerly position of the Azores high-pressure system (Supplementary Fig. S5).

The above-mentioned recent weather situations that triggered droughts or floods in the Alpine region (Central Europe) support our finding of less (more) intense precipitation events during warmer (cooler) summers accompanied by a strong (weak) high-pressure systems dominating Europe during the past 2500 years.

References

32. Simmons, A., Uppala, S., Dee, D. & Kobayashi, S. ERA-Interim: New ECMWF reanalysis product form 1989 onward. (*ECMWF Newsletter*, **110,** Winter 2006/2007). Data can be downloaded from www.ecmwf.int/products/data.

33. Gridded precipitation/daily sum@MeteoSwiss; swisstopo (Art. 30 GeoIV): 5704 000 000 / vector200@2010, reproduced with permission of swisstopo / JA100119.

34. Reimer, P. J. *et al.* Intcal09 and Marine09 radiocarbon age calibration curves, 0–50,000 years cal BP. *Radiocarbon* **51,** 1111-1150 (2009).

35. Beniston, M. The 2003 heat wave in Europe: A shape of things to come? An analysis based on Swiss climatological data and model simulations. *Geophys. Res.* Lett. **31,** L02202 (2004).

36. Coumou, D. & Rahmstorf, S. A decade of weather extremes. *Nature Clim. Change* **2,** 491-496 (2012).

37. Rickenmann, D. & Koschni, A. Sediment loads due to fluvial transport and debris flows during the 2005 flood events in Switzerland. *Hydrol. Process.* **24,** 993-1007 (2010).